OTFS and Delay Doppler Communications

Tutorial - Symposium - SCSS - APCC2022

A/Prof Yi Hong

Department of Electrical and Computer Systems Engineering
Monash University, Clayton, Australia

Overview I

Overview II

4. OTFS Signal Detection

5. OTFS channel estimation

6. OTFS application

Links to download Matlab code:

https://ecse.monash.edu/staff/eviterbo/OTFS-VTC18/OTFS%20MRC%20detection%20MATLAB%20code.zip

https://ecse.monash.edu/staff/eviterbo/OTFS-VTC18/OTFS_sample_code.zip

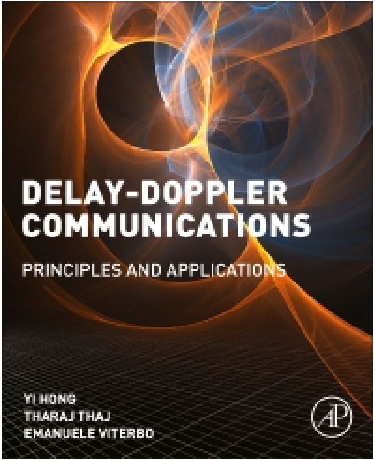

* Y. Hong, T. Thaj, and E. Viterbo, *Delay-Doppler Communications: Principles and Applications.* Academic Press - Elsevier, 2/2022, ISBN:9780323850285

News

IEEE ComSoc Online Course:

OTFS and Delay-Doppler Communications

16 - 17 November 2022, 2:00 pm to 6:00 pm EST

E. Viterbo (Instructor), Y. Hong and T. Thaj (Developers)

Link: `https://www.comsoc.org/education-training/training-courses/online-courses/2022-11-otfs-and-delay-doppler-communications`

Book: Y. Hong, T. Thaj, and E. Viterbo, *Delay-Doppler Communications: Principles and Applications.* Academic Press - Elsevier, 2/2022, ISBN:9780323850285

Introduction

Evolution of wireless

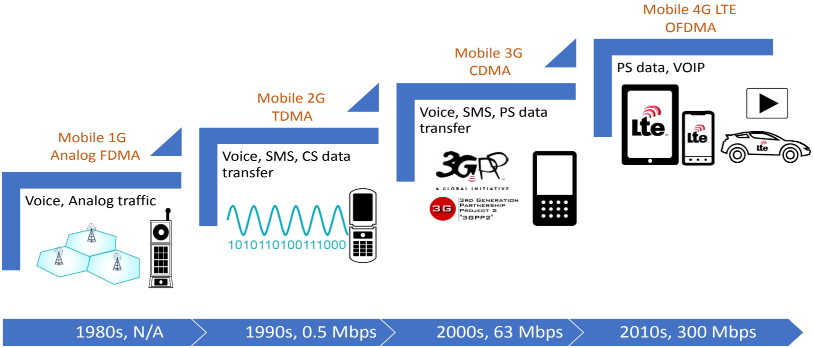

- Waveform design is the major change between the generations

High-Doppler wireless channels

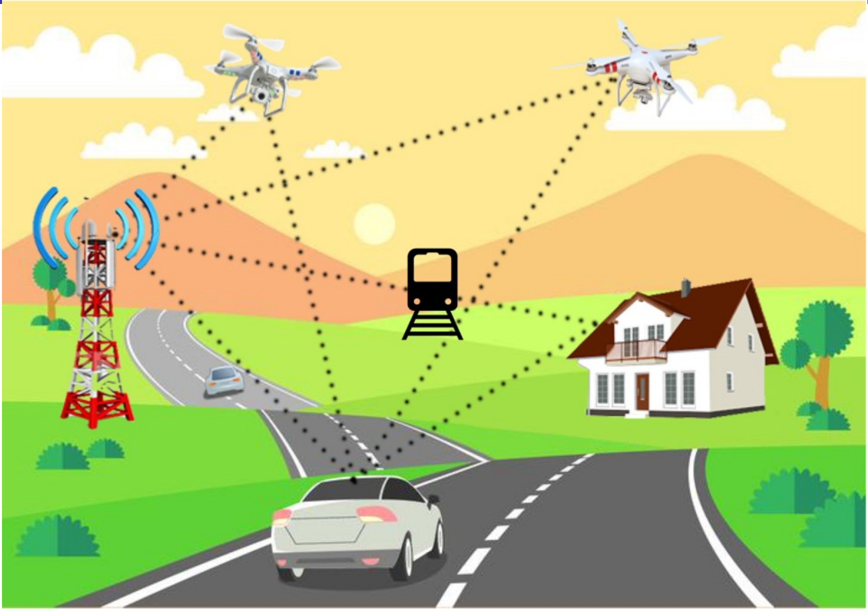

Wireless Channels - delay spread

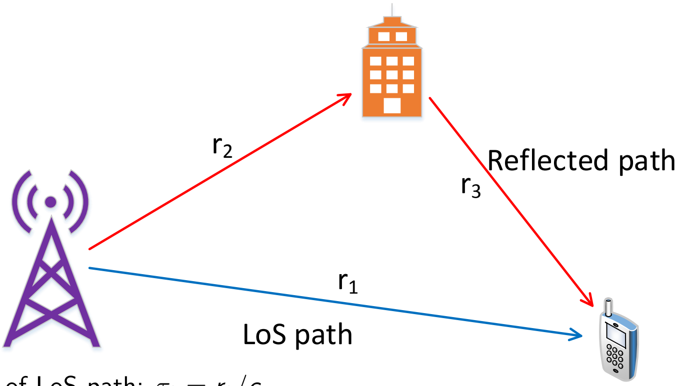

- Delay of LoS path: $\tau_1 = r_1/c$
- Delay of reflected path: $\tau_2 = (r_2 + r_3)/c$
- Delay spread: $\tau_2 - \tau_1$
- Received signal:

$$r(t) = h_1 \underbrace{s(t-\tau_1)}_{\text{delay}} + h_2 \underbrace{s(t-\tau_2)}_{\text{delay}}$$

Wireless Channels - Doppler spread

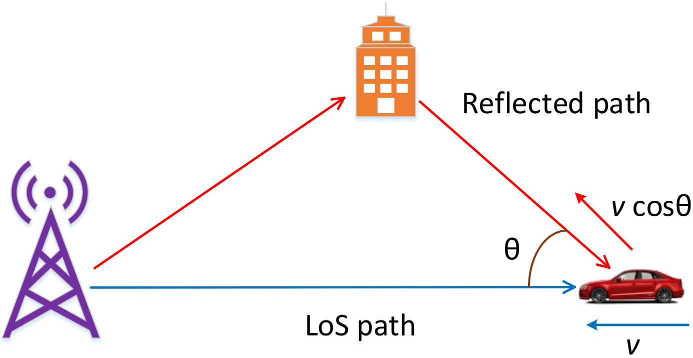

- Doppler frequency of LoS path: $\nu_1 = f_c \frac{v}{c}$
- Doppler frequency of reflected path: $\nu_2 = f_c \frac{v \cos\theta}{c}$
- Doppler spread: $\nu_2 - \nu_1$
- Received signal:

$$r(t) = h_1 \underbrace{e^{j2\pi\nu_1(t-\tau_1)}}_{\text{Doppler}} \underbrace{s(t-\tau_1)}_{\text{delay}} + h_2 \underbrace{e^{j2\pi\nu_2(t-\tau_2)}}_{\text{Doppler}} \underbrace{s(t-\tau_2)}_{\text{delay}}$$

Typical delay and Doppler spreads

Delay spread ($c = 3 \cdot 10^8$m/s)

$\Delta r_{\max}$	Indoor (3m)	Outdoor (3km)
$\tau_{\max}$	10ns	10μs

Doppler spread

$\nu_{\max}$	$f_c = 2$GHz	$f_c = 60$GHz
$v = 1.5$m/s $= 5.5$km/h	10Hz	300Hz
$v = 3$m/s $= 11$km/h	20Hz	600Hz
$v = 30$m/s $= 110$km/h	200Hz	6KHz
$v = 150$m/s $= 550$km/h	1KHz	30KHz

Wireless Channels: time domain

- Consider P propagation paths with parameters: (h_i, τ_i, ν_i), $i = 1, \ldots, P$

$$r(t) = \sum_{i=1}^{P} \underbrace{h_i e^{j2\pi\nu_i(t-\tau_i)}}_{g(t,\tau_i)} s(t-\tau_i)$$

- Received signal in terms of time-varying convolution

$$r(t) = \int \underbrace{g(t,\tau)}_{\text{time-variant impulse response}} s(t-\tau) d\tau$$

where the time-variant impulse response

$$g(t,\tau) = \sum_{i=1}^{P} h_i e^{j2\pi\nu_i(t-\tau_i)} \delta(\tau-\tau_i)$$

Time-variant impulse response $g(t, \tau)$

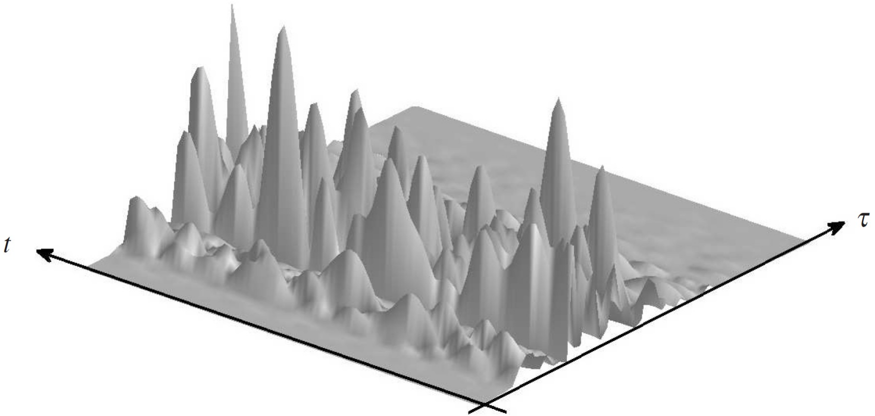

* G. Matz and F. Hlawatsch, *Chapter 1, Wireless Communications Over Rapidly Time-Varying Channels.* New York, NY, USA: Academic, 2011

OFDM

- OFDM - Orthogonal Frequency Division Multiplexing

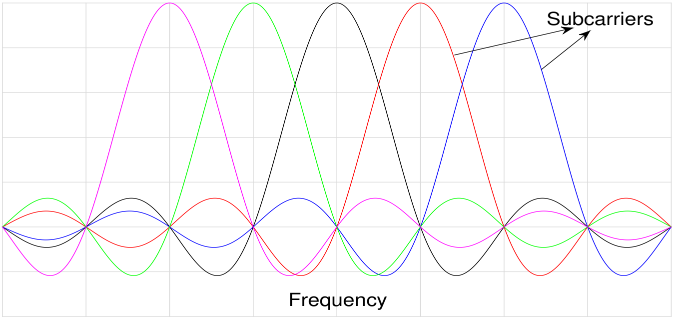

- OFDM divides the frequency selective channel into multiple parallel sub-channels

OFDM system model

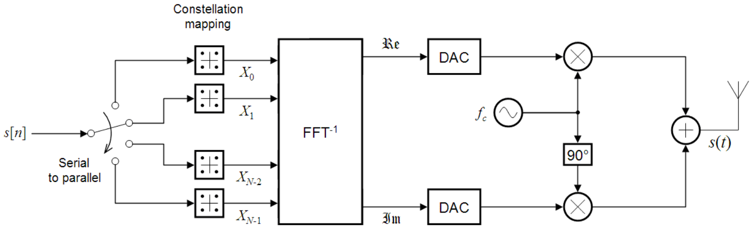

Figure: OFDM Tx

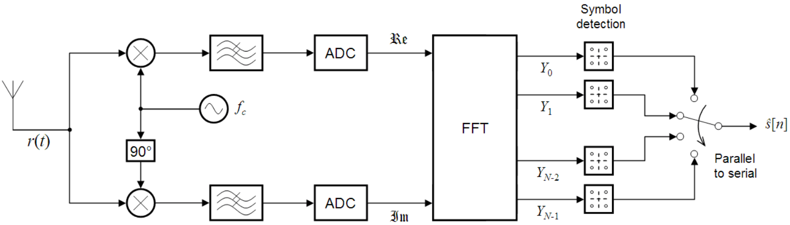

Figure: OFDM Rx

(*) From Wikipedia, the free encyclopedia

Effect of high multiple Dopplers in OFDM

- Introduces inter carrier interference (ICI)

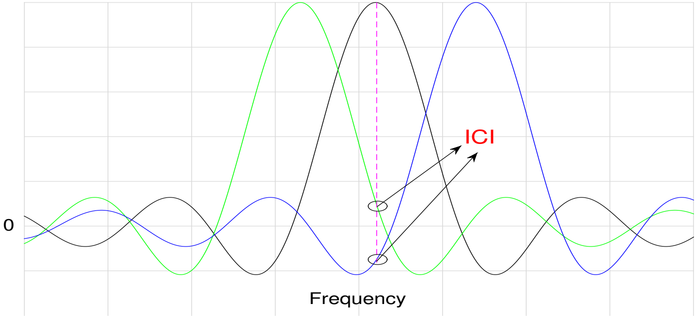

OTFS

- Orthogonal Time Frequency Space Modulation (OTFS)(*)
  - Solves the two cons of OFDM
  - Works in Delay–Doppler domain rather than Time–Frequency domain

(*) R. Hadani, S. Rakib, M. Tsatsanis, A. Monk, A. J. Goldsmith, A. F. Molisch, and R. Calderbank, "Orthogonal time frequency space modulation," in *Proc. IEEE WCNC*, San Francisco, CA, USA, March 2017.

Wireless channel representation

- Different representations of linear time variant (LTV) wireless channels

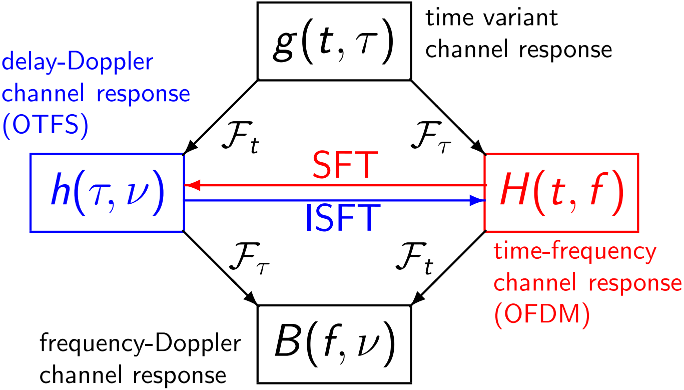

Figure: Different domain representations of a time-variant multipath channel impulse response $g(t,\tau)$, also denoted as the delay-time channel response

Wireless channel representation

- The received signal in linear time variant channel (LTV)

$$r(t) = \int \underbrace{g(t,\tau)}_{\text{time-variant impulse response}} s(t-\tau)d\tau \rightarrow \text{generalization of LTI}$$

$$= \int\int \underbrace{h(\tau,\nu)}_{\text{Delay–Doppler spreading function}} s(t-\tau)e^{j2\pi\nu t}d\tau d\nu \rightarrow \text{Delay–Doppler Channel}$$

$$= \int \underbrace{H(t,f)}_{\text{time-frequency response}} S(f)e^{j2\pi ft}df \rightarrow \text{Time–Frequency Channel}$$

- Relation between Delay-Doppler channel response $h(\tau,\nu)$ and time-frequency channel response $H(t,f)$

$$\left.\begin{aligned} h(\tau,\nu) &= \int\int H(t,f)e^{-j2\pi(\nu t - f\tau)}dtdf \\ H(t,f) &= \int\int h(\tau,\nu)e^{j2\pi(\nu t - f\tau)}d\tau d\nu \end{aligned}\right\} \text{Pair of } \textbf{2D symplectic FT}$$

Wireless channel representation

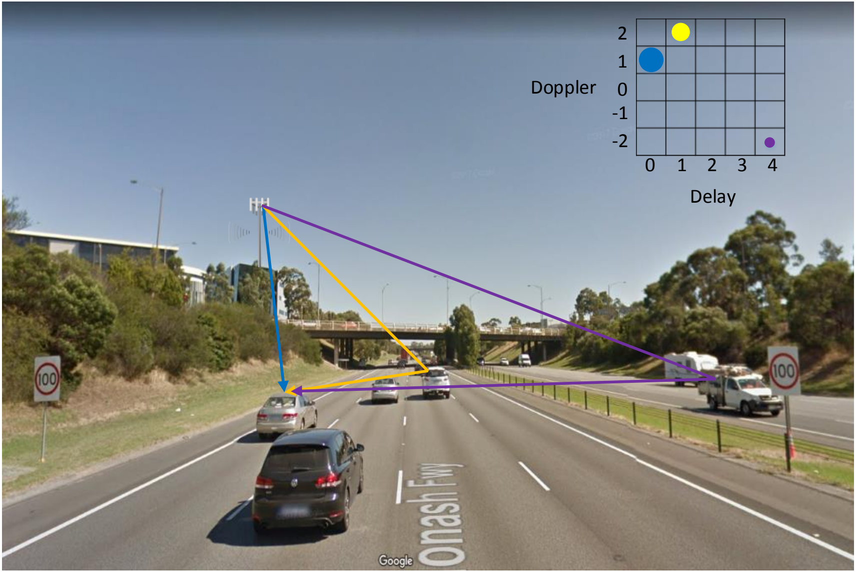

Wireless channel representation

High mobility multipath channel in delay-Doppler domain

- Received signal in terms of the delay-Doppler channel

$$r(t) = \int\int \underbrace{h(\tau,\nu)}_{\text{Delay–Doppler channel response}} s(t-\tau) e^{j2\pi\nu t} d\tau d\nu$$

where the delay-Doppler response of a multipath channel of P paths with parameters (h_i, τ_i, ν_i), $i = 1, \ldots, P$

$$h(\tau,\nu) = \sum_{i=1}^{P} \underbrace{h_i e^{-j2\pi\tau_i\nu_i}}_{h_i'} \delta(\tau - \tau_i)\delta(\nu - \nu_i)$$

- This leads to

$$r(t) = \sum_{i=1}^{P} \underbrace{h_i e^{-j2\pi\nu_i\tau_i}}_{\text{gain}} \underbrace{e^{j2\pi\nu_i t}}_{\text{Doppler}} \underbrace{s(t-\tau_i)}_{\text{delay}}$$

Delay-Doppler $h(\tau, \nu)$ vs Time-frequency $H(t, f)$ channel

Multipath mobile channel

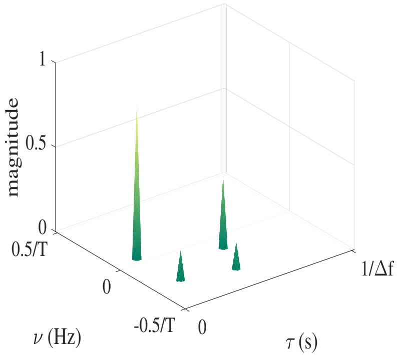

(a) $h(\tau, \nu)$

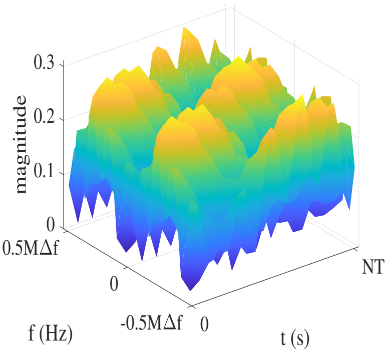

(b) $H(t, f)$

Figure: The continuous delay-Doppler vs time-frequency channel representation of a high mobility multipath channel (linear time-varying)

Discrete baseband equivalent channel

- Let the Tx signal $s(t)$ be of bandwidth $B = M\Delta f$ [Hz] and duration $T_f = NT$ [s], and $T\Delta f = 1$.
- Let the baseband Rx sampling rate $f_s = 1/T_s = B$ [Hz]
- Discrete-time signals sampled at sampling interval $T_s = 1/B = T/M$ [s].

$$s[n] = s(t)|_{t=nT_s}, \quad r[n] = r(t)|_{t=nT_s}$$

- The discrete-time baseband channel for $l, n \in \mathbb{Z}$

$$g^{\mathrm{s}}[l,n] = g(\tau, t)|_{\tau=lT_s, t=nT_s}$$

- Received discrete baseband signal

$$r[n] = \sum_{l} g^{\mathrm{s}}[l,n] s[n-l]$$

Time–Frequency and delay–Doppler grids

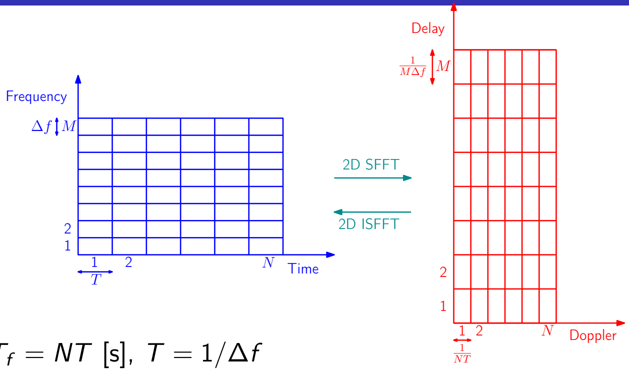

- $B = M\Delta f$, $T_f = NT$ [s], $T = 1/\Delta f$
- delay resolution $T/M = T_s$, Doppler resolution $\Delta f/N = 1/T_f = 1/NT$
- Delay-Doppler channel response

$$h(\tau, \nu) = \sum_{i=1}^{P} h'_i \delta(\tau - \tau_i)\delta(\nu - \nu_i)$$

- Assume $\tau_i = l_i \left(\frac{1}{M\Delta f}\right)$ and $\nu_i = k_i \left(\frac{1}{NT}\right)$, $l_i, k_i \in \mathbb{Z}$

$$h[l, k] = \begin{cases} h'_i & \text{if } l = l_i, \ k = k_i \\ 0 & \text{otherwise} \end{cases}$$

OTFS modulation

OTFS modulation by Hadani'17

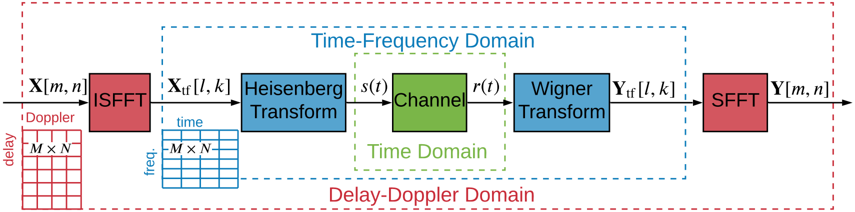

Figure: OTFS mod/demod

- OTFS is equivalent to OFDM with 2-D unitary precoding (ISFFT) in the time-frequency domain, which spreads each information symbol equally in M sub-carriers and N time-slots.

- Received signal in delay–Doppler domain

$$
\begin{aligned}
y[k,l] &= \sum_{i=1}^{P} h_i x[[k-k_{\nu_i}]_N, [l-l_{\tau_i}]_M] \\
&= h[k,l] \circledast x[k,l] \qquad \text{(2D Circular Convolution)}
\end{aligned}
$$

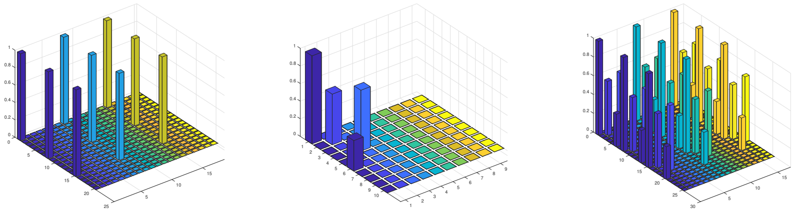

(a) Input signal, $x[k,l]$ (b) Channel, $h[k,l]$ (c) Output signal, $y[k,l]$

Figure: OTFS signals

OTFS with ideal vs rectangular pulses – time–frequency domain

- Time–frequency input-output relation with ideal pulses

$$\mathbf{Y}_{\mathrm{tf}}[k,l] = \mathbf{H}_{\mathrm{tf}}[k,l]\mathbf{X}_{\mathrm{tf}}[k,l]$$

- Time–frequency input-output relation with rectangular pulses

$$\mathbf{Y}_{\mathrm{tf}}[k,l] = \mathbf{H}_{\mathrm{tf}}[k,l]\mathbf{X}_{\mathrm{tf}}[k,l] + \mathsf{ICI} + \mathsf{ISI}$$

- ICI – loss of orthogonality in frequency domain due to Dopplers
- ISI – loss of orthogonality in time domain due to delays

(*) P. Raviteja, K. T. Phan, Y. Hong, and E. Viterbo, "Interference cancellation and iterative detection for orthogonal time frequency space modulation," *IEEE Trans. Wireless Commun.*, vol. 17, no. 10, pp. 6501-6515, Oct. 2018.

Rectangular pulses

- Rectangular pulses:
  - TF I/O relation: ISI and ICI due to delay and Doppler spread

$$\mathbf{Y}_{\mathrm{tf}}[k,l] = \mathbf{H}_{\mathrm{tf}}[k,l]\mathbf{X}_{\mathrm{tf}}[k,l] + \mathrm{ICI} + \mathrm{ISI}$$

  - DD I/O relation: 2-D twisted circular convolution

$$\mathbf{Y}[k,l] = \sum_{i=1}^{P} h_i \alpha(k,l,k_i,l_i)\mathbf{X}[[k-k_i]_N, [l-l_i]_M]$$

where $\alpha(k,l,k_i,l_i) = e^{\frac{j2\pi k_i(l-l_i)}{NM}} e^{j\frac{2\pi}{N}(k-k_i)\left\lfloor\frac{l-l_i}{M}\right\rfloor}$ are the phase rotations due to ICI and ISI ($\lfloor\cdot\rfloor$ denotes the floor operation). They are associated with channel delay and Doppler indices (k_i, l_i) and symbol location (k, l) in the DD grid, which can be easily corrected.

OTFS Input-Output Relation in Matrix Form

OTFS transmitter implementation: $M = 2048,\ N = 128$

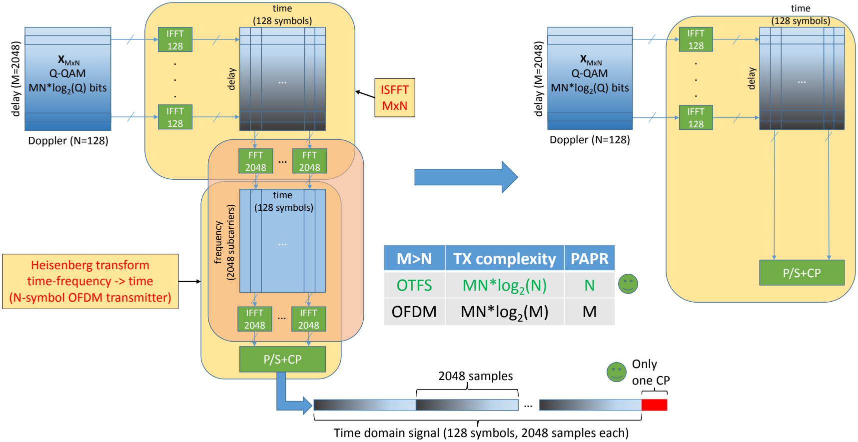

M>N	TX complexity	PAPR
OTFS	MN*log$_2$(N)	N
OFDM	MN*log$_2$(M)	M

- When the sizes of the FFT in ISFFT and the IFFT in Heisenberg transform are the same, then the LHS structure reduces to the RHS one, which is the inverse ZAK transform

OTFS modulation: Matrix form

- Tx signal in time domain: ISFFT (DD-TF) + Heisenberg (TF-T)

$$\text{Matrix form } \mathbf{S} = \mathbf{G}_{\text{tx}}\mathbf{F}_M^\dagger \underbrace{\mathbf{F}_M\mathbf{X}\mathbf{F}_N^\dagger}_{\text{ISFFT}} = \mathbf{G}_{\text{tx}} \underbrace{\mathbf{X}\mathbf{F}_N^\dagger}_{\tilde{\mathbf{X}}}$$

$$\text{Vector form } \mathbf{s} = \text{vec}(\mathbf{S}) = \text{vec}(\mathbf{G}_{\text{tx}} \underbrace{\mathbf{X}\mathbf{F}_N^\dagger}_{\tilde{\mathbf{X}}})$$

- For rectangular pulse shaping waveforms ($\mathbf{G}_{\text{tx}} = \mathbf{I}_M$):

$$\mathbf{S} = \mathbf{X}\mathbf{F}_N^\dagger = \tilde{\mathbf{X}} \qquad \mathbf{s} = \text{vec}(\mathbf{X}\mathbf{F}_N^\dagger) = \text{vec}(\tilde{\mathbf{X}})$$

- The above operation is equivalent to the well known inverse discrete Zak transform (IDZT)

$$\mathbf{s} = \text{IDZT}\{\mathbf{X}\} = \text{vec}(\mathbf{X}\mathbf{F}_N^\dagger)$$

OTFS Tx implementation: $M = 2048$, $N = 128$

- Tx does the inverse discrete ZAK transform:

$$\mathbf{s} = \boxed{\text{IDZT}\{\mathbf{X}\}} = \text{vec}(\mathbf{X}\mathbf{F}_N^{\dagger})$$

  when the sizes of the FFT in ISFFT and the IFFT in Heisenberg transform are the same.

- The simplified Tx structure is equivalent to V-OFDM(*) [a.k.a. A-OFDM†], proposed for static multipath channels only(**), but Not investigated for high mobility communications.

(*) X. Xia, "Precoded and vector OFDM robust to channel spectral nulls and with reduced cyclic prefix length in single transmit antenna systems", in *IEEE Trans. on Commun.*, 2001.
($\dagger$) J. Zhang, A. Jayalath, Y. Chen, "Asymmetric OFDM Systems Based on Layered FFT Structure", in *IEEE Signal Processing Letters*, 2007.
(**) P.Raviteja, E.Viterbo, Y. Hong, "OTFS Performance on Static Multipath Channels", in *IEEE Wireless Communications Letters*, 2019.

OTFS demodulation: Matrix form

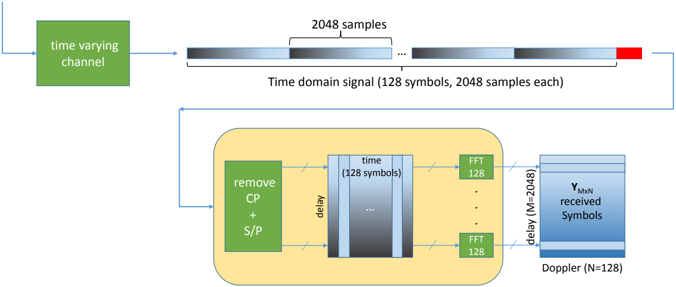

- Rx signal in delay-Doppler domain: Wigner (T-TF) + SFFT (TF-DD)

$$\mathbf{Y} = \mathbf{F}_M^\dagger \mathbf{F}_M \mathbf{G}_{\mathrm{rx}} \underbrace{\mathrm{vec}_{M,N}^{-1}(\mathbf{r})}_{\widetilde{\mathbf{Y}}} \mathbf{F}_N = \mathbf{G}_{\mathrm{rx}} \widetilde{\mathbf{Y}} \mathbf{F}_N$$

- For rectangular pulse shaping waveforms $(\mathbf{G}_{\mathrm{rx}} = \mathbf{I}_M)$: $\mathbf{Y} = \widetilde{\mathbf{Y}} \cdot \mathbf{F}_N$
- It is equivalent to the discrete Zak transform (DZT)

$$\mathbf{Y} = \mathrm{DZT}\{\mathbf{r}\} = \mathrm{vec}_{M,N}^{-1}(\mathbf{r}) \cdot \mathbf{F}_N = \widetilde{\mathbf{Y}} \cdot \mathbf{F}_N$$

OTFS demodulation: Matrix form

- Tx and Rx are operating inverse discrete Zak and discrete Zak Transforms, respectively.

(*) S.K Mohammed, "Derivation of OTFS Modulation From First Principles," *IEEE Trans. on Veh. Tech.*, vol. 70, no.8, pp. 7619-7636, Aug. 2021.

(*) Y. Hong, T. Thaj, and E. Viterbo, *Delay-Doppler Communications: Principles and Applications*, Academic Press, an imprint of Elsevier, Feb. 2022.

OTFS: matrix representation – channel

- Received signal in vector form in time domain (assuming noiseless)

$$\mathbf{r} = \mathbf{G}\mathbf{s}$$

- $\mathbf{G}$ is an $MN \times MN$ matrix of the following form

$$\mathbf{G} = \sum_{i=1}^{P} h_i' \mathbf{\Pi}^{l_i} \mathbf{\Delta}^{(k_i)},$$

where, $\mathbf{\Pi}$ is the permutation matrix (forward cyclic shift), and $\mathbf{\Delta}^{(k_i)}$ is the diagonal matrix

$$\underbrace{\mathbf{\Pi} = \begin{bmatrix} 0 & \cdots & 0 & 1 \\ 1 & \ddots & 0 & 0 \\ \vdots & \ddots & \ddots & \vdots \\ 0 & \cdots & 1 & 0 \end{bmatrix}_{MN \times MN}}_{\text{Delay (similar to OFDM)}}, \underbrace{\mathbf{\Delta}^{(k_i)} = \begin{bmatrix} e^{\frac{j2\pi k_i(0)}{MN}} & 0 & \cdots & 0 \\ 0 & e^{\frac{j2\pi k_i(1)}{MN}} & \cdots & 0 \\ \vdots & & \ddots & \vdots \\ 0 & 0 & \cdots & e^{\frac{j2\pi k_i(MN-1)}{MN}} \end{bmatrix}}_{\text{Doppler}}$$

Summary of OTFS Channel matrix representation

- The $MN \times MN$ channel matrix for rectangular pulses:

$$\mathbf{H} = \sum_{i=1}^{P} h_i' \underbrace{\left[(\mathbf{F}_N \otimes \mathbf{I}_M)\mathbf{\Pi}^{l_i}(\mathbf{F}_N^H \otimes \mathbf{I}_M)\right]}_{\mathbf{P}^{(i)} \text{ (delay)}} \underbrace{\left[(\mathbf{F}_N \otimes \mathbf{I}_M)\mathbf{\Delta}^{(k_i)}(\mathbf{F}_N^H \otimes \mathbf{I}_M)\right]}_{\mathbf{Q}^{(i)} \text{ (Doppler)}}$$

$$= \sum_{i=1}^{P} h_i' \mathbf{P}^{(i)} \mathbf{Q}^{(i)} = \boxed{\sum_{i=1}^{P} h_i' \mathbf{T}^{(i)}}$$

- $\mathbf{T}^{(i)}$ has only one non-zero element in each row and the position and value of the non-zero element depends on the delay and Doppler values.
- The channel matrix **H** has only P nonzero entries in each row and column, i.e., a simple sparse structure.

*P. Raviteja, Y. Hong, E. Viterbo, and E. Biglieri, "Practical pulse-shaping waveforms for reduced-cyclic-prefix OTFS," *IEEE Trans. Veh. Technol.*, vol. 68, no. 1, pp. 957-961, 2019.

OTFS: Example for computing $\mathbf{H}_{\text{eff}}^{\text{rect}}$

- $M = 2,\ N = 2, MN = 4$
- $l_i = 0$ and $k_i = 0$ (no delay and Doppler)
  - $\mathbf{\Pi}^{l_i=0} = \mathbf{I}_4 \Rightarrow \mathbf{P}^{(i)} = (\mathbf{F}_2 \otimes \mathbf{I}_2)(\mathbf{F}_2^H \otimes \mathbf{I}_2) = \mathbf{I}_4$
  - $\mathbf{\Delta}^{(k_i=0)} = \mathbf{I}_4 \Rightarrow \mathbf{Q}^{(i)} = (\mathbf{F}_2 \otimes \mathbf{I}_2)(\mathbf{F}_2^H \otimes \mathbf{I}_2) = \mathbf{I}_4$
  - $\mathbf{T}^{(i)} = \mathbf{P}^{(i)}\mathbf{Q}^{(i)} = \mathbf{I}_4 \Rightarrow$ Narrowband channel

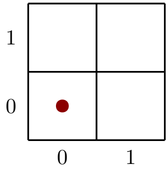

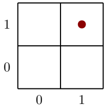

- $l_i = 1$ and $k_i = 1$ (both delay and Doppler)
  - $\mathbf{P}^{(i)} = \begin{bmatrix} 0 & 1 & 0 & 0 \\ 1 & 0 & 0 & 0 \\ 0 & 0 & 0 & e^{-j2\pi\frac{1}{2}} \\ 0 & 0 & 1 & 0 \end{bmatrix}$
  - $\mathbf{Q}^{(i)} = \begin{bmatrix} 0 & 0 & 1 & 0 \\ 0 & 0 & 0 & e^{j2\pi\frac{1}{4}} \\ 1 & 0 & 0 & 0 \\ 0 & e^{j2\pi\frac{1}{4}} & 0 & 0 \end{bmatrix}$
  - $\mathbf{T}^{(i)} = \mathbf{P}^{(i)}\mathbf{Q}^{(i)} \Rightarrow \mathbf{T}^{(i)}\mathbf{s} \rightarrow$ circularly shifts both the blocks (size M) and the elements in each block of $\mathbf{s}$ by 1 (delay and Doppler shifts)

OTFS: channel for rectangular pulses

- $\mathbf{T}^{(i)}$ has only one non-zero element in each row and the position and value of the non-zero element depends on the delay and Doppler values.

$$\mathbf{T}^{(i)}(p,q) = \begin{cases} e^{-j2\pi\frac{n}{N}} e^{j2\pi\frac{k_i([m-l_i]_M)}{MN}}, & \text{if } q = [m-l_i]_M + M[n-k_i]_N \text{ and } m < l_i \\ e^{j2\pi\frac{k_i([m-l_i]_M)}{MN}}, & \text{if } q = [m-l_i]_M + M[n-k_i]_N \text{ and } m \geq l_i \\ 0, & \text{otherwise.} \end{cases}$$

- Example: $l_i = 1$ and $k_i = 1$

$$\mathbf{T}^{(i)} = \begin{bmatrix} 0 & 0 & 0 & e^{j2\pi\frac{1}{4}} \\ 0 & 0 & 1 & 0 \\ 0 & e^{-j2\pi\frac{1}{4}} & 0 & 0 \\ 1 & 0 & 0 & 0 \end{bmatrix}$$

MIMO-OTFS Input-Output Relation in Matrix Form

MIMO-OTFS modulation

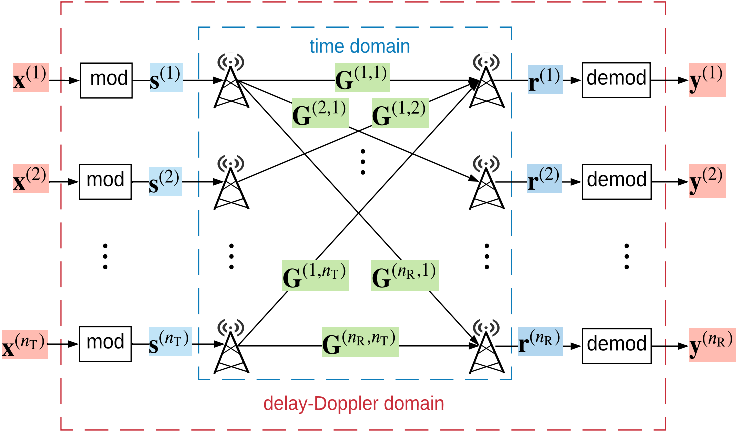

Figure: Block diagram of MIMO-OTFS modulation scheme

* T. Thaj and E. Viterbo, "Low-Complexity Linear Diversity-Combining Detector for MIMO-OTFS", in *IEEE Wireless Commun. Lett.*, vol. 11, no. 2, pp. 288-292, Feb. 2022.

Delay-Doppler input-output relation

- MIMO-OTFS time domain input-output relation:

$$\mathbf{r}_{\mathrm{MIMO}} = \mathbf{G}_{\mathrm{MIMO}} \cdot \mathbf{s}_{\mathrm{MIMO}}$$

where $\mathbf{r}_{\mathrm{MIMO}} \in \mathbb{C}^{n_R MN}$, $\mathbf{s}_{\mathrm{MIMO}} \in \mathbb{C}^{n_T MN}$ are the received and transmitted signal samples vector and

$$\mathbf{G}_{\mathrm{MIMO}} \in \mathbb{C}^{n_R MN \times n_T MN} = \begin{bmatrix} \mathbf{G}^{(1,1)} & \dots & \mathbf{G}^{(1,n_T)} \\ \vdots & \ddots & \vdots \\ \mathbf{G}^{(n_R,1)} & \dots & \mathbf{G}^{(n_R,n_T)} \end{bmatrix}$$

is the MIMO-OTFS channel matrix with each submatrix $\mathbf{G}^{(r,t)} \in \mathbb{C}^{MN \times MN}$ as

$$\mathbf{G}^{(r,t)} = \sum_{i=1}^{P} h_i' \mathbf{\Pi}^{l_i} \mathbf{\Delta}^{(k_i)}, \quad t = 1, \dots, n_T, \; r = 1, \dots, n_R.$$

MIMO-OTFS delay Doppler domain input-output relation

- MIMO-OTFS delay-Doppler domain input-output relation:

$$\underbrace{\begin{bmatrix} \mathbf{y}^{(1)} \\ \mathbf{y}^{(2)} \\ \vdots \\ \mathbf{y}^{(n_{\mathrm{R}})} \end{bmatrix}}_{\mathbf{y}_{\mathrm{MIMO}}} = \underbrace{\begin{bmatrix} \mathbf{H}^{(1,1)} & \mathbf{H}^{(1,2)} & \dots & \mathbf{H}^{(1,n_{\mathrm{T}})} \\ \mathbf{H}^{(2,1)} & \mathbf{H}^{(2,2)} & \dots & \mathbf{H}^{(2,n_{\mathrm{T}})} \\ \vdots & \ddots & \ddots & \vdots \\ \mathbf{H}^{(n_{\mathrm{R}},1)} & \mathbf{H}^{(n_{\mathrm{R}},2)} & \dots & \mathbf{H}^{(n_{\mathrm{R}},n_{\mathrm{T}})} \end{bmatrix}}_{\mathbf{H}_{\mathrm{MIMO(NMn_R \times NMn_T})}} \underbrace{\begin{bmatrix} \mathbf{x}^{(1)} \\ \mathbf{x}^{(2)} \\ \vdots \\ \mathbf{x}^{(n_{\mathrm{T}})} \end{bmatrix}}_{\mathbf{x}_{\mathrm{MIMO}}}$$

- The terms $\mathbf{y}_{\mathrm{MIMO}} \in \mathbb{C}^{n_R MN}$ and $\mathbf{x}_{\mathrm{MIMO}} \in \mathbb{C}^{n_T MN}$ are the received and transmitted time-domain signal samples vectors.
- The delay-Doppler domain channel matrix $\mathbf{H}_{\mathrm{MIMO}}$ has submatrices $\mathbf{H}^{(r,t)} \in \mathbb{C}^{MN \times MN}$ for $r = 1, \dots, n_R$ and $t = 1, \dots, n_T$.

OTFS Signal Detection

Vectorized formulation of the input-output relation

- The input-output relation in the DD domain is a 2D twisted convolution

$$\mathbf{Y}[k,l] = \sum_{i=1}^{P} h_i \alpha(k,l,k_i,l_i) \mathbf{X}[[k-k_i]_N, [l-l_i]_M] + \mathbf{W}[k,l]$$

where $m = 1 \dots M, n = 1 \dots N$.

- We can reorganize the above equation in the vectorized form as

$$\mathbf{y} = \underbrace{\mathbf{H}}_{NM \times NM} \mathbf{x} + \mathbf{w} \tag{1}$$

where $\mathbf{x} \in \mathbb{C}^{NM}$, $\mathbf{y} \in \mathbb{C}^{NM}$ are the transmitted symbol vector and the received signal samples vector, and $\mathbf{H}$ is the DD domain channel matrix and has only P non-zero terms in each row.

- Given the sparse nature of $\mathbf{H}$ we can solve (1) by using a message passing algorithm

Message passing based detection

- Symbol-by-symbol MAP detection for $c = 1, \ldots, NM$

$$
\begin{aligned}
\widehat{x}[c] &= \arg\max_{a_j \in \mathbb{A}} \Pr\left(x[c] = a_j \,\middle|\, \mathbf{y}, \mathbf{H}\right) \\
&= \arg\max_{a_j \in \mathbb{A}} \frac{1}{Q} \Pr\left(\mathbf{y} \,\middle|\, x[c] = a_j, \mathbf{H}\right) \\
&\approx \arg\max_{a_j \in \mathbb{A}} \prod_{d \in \mathcal{J}_c} \Pr\left(y[d] \,\middle|\, x[c] = a_j, \mathbf{H}\right)
\end{aligned}
$$

- Received signal $y[d]$

$$
y[d] = x[c]H[d,c] + \underbrace{\sum_{e \in \mathcal{I}_d, e \neq c} x[e]H[d,e] + z[d]}_{\zeta_{d,c}^{(i)} \rightarrow \text{ assumed to be Gaussian}}
$$

Messages in factor graph

Algorithm MP algorithm for OTFS symbol detection

Input: Received signal $\mathbf{y}$, channel matrix $\mathbf{H}$

Initialization: pmf $\mathbf{p}_{c,d}^{(0)} = 1/Q$ **repeat**

- Observation nodes send the mean and variance to variable nodes
- Variable nodes send the pmf to the observation nodes
- Update the decision

until *Stopping criteria*;

Output: The decision on transmitted symbols $\widehat{x}[c]$

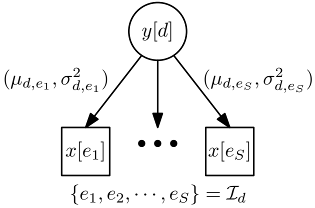

Observation node messages

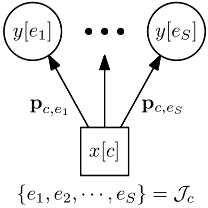

Variable node messages

Messages in factor graph – observation node messages

- Received signal

$$y[d] = x[c]H[d,c] + \underbrace{\sum_{e \in \mathcal{I}(d), e \neq c} x[e]H[d,e] + z[d]}_{\zeta_{d,c}^{(i)} \rightarrow \text{ assumed to be Gaussian}}$$

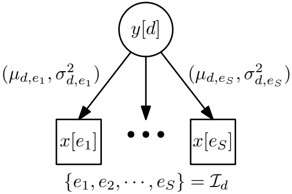

- Mean and Variance

$$\mu_{d,c}^{(i)} = \sum_{e \in \mathcal{I}(d), e \neq c} \sum_{j=1}^{Q} p_{e,d}^{(i-1)}(a_j) a_j H[d,e]$$

$$(\sigma_{d,c}^{(i)})^2 = \sum_{e \in \mathcal{I}(d), e \neq c} \left(\sum_{j=1}^{Q} p_{e,d}^{(i-1)}(a_j) |a_j|^2 |H[d,e]|^2 - \left| \sum_{j=1}^{Q} p_{e,d}^{(i-1)}(a_j) a_j H[d,e] \right|^2 \right) + \sigma^2$$

Messages in factor graph – variable node messages

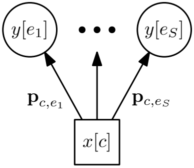

- Probability update with damping factor Δ

$$p_{c,d}^{(i)}(a_j) = \Delta \cdot \tilde{p}_{c,d}^{(i)}(a_j) + (1 - \Delta) \cdot p_{c,d}^{(i-1)}(a_j), a_j \in \mathbb{A}$$

where

$$\tilde{p}_{c,d}^{(i)}(a_j) \propto \prod_{e \in \mathcal{J}(c), e \neq d} \Pr\left(y[e] \middle| x[c] = a_j, \mathbf{H}\right)$$

$$= \prod_{e \in \mathcal{J}(c), e \neq d} \frac{\xi^{(i)}(e, c, j)}{\sum_{k=1}^{Q} \xi^{(i)}(e, c, k)}$$

$$\xi^{(i)}(e, c, k) = \exp\left(\frac{-\left|y[e] - \mu_{e,c}^{(i)} - H_{e,c} a_k\right|^2}{(\sigma_{e,c}^{(i)})^2}\right)$$

Final update and stopping criterion

- Final update

$$p_c^{(i)}(a_j) = \prod_{e \in \mathcal{J}(c)} \frac{\xi^{(i)}(e,c,j)}{\sum_{k=1}^{Q} \xi^{(i)}(e,c,k)}$$

$$\widehat{x}[c] = \arg\max_{a_j \in \mathbb{A}} \; p_c^{(i)}(a_j), \quad c = 1, \cdots, NM.$$

- Stopping Criterion
  - Convergence Indicator $\eta^{(i)} = 1$

$$\eta^{(i)} = \frac{1}{NM} \sum_{c=1}^{NM} \mathbb{I}\left(\max_{a_j \in \mathbb{A}} \; p_c^{(i)}(a_j) \geq 0.99 \right)$$

  - Maximum number of Iterations
- Complexity – $\mathcal{O}(NMPQ)$ per iteration

Other detection methods

- *MRC detection (Ref[c])*
- MMSE detection (Ref [23][24])
- FDE (frequency domain equalization) (Ref [19])
- OTFS MMSE-PIC (Ref [20])
- MP algorithm variants and improvements (Ref [43]-[47])
- neural network based detection (Ref [48]-[50])
- A detailed OTFS detection surveys can be found in References [a] and [b].

---

[a]. Z. Q. Zhang, H. Liu, Q. L. Wang, and P. Fan, "A survey on low complexity detectors for OTFS systems," ZTE Communications, vol. 19, no. 4, pp. 03–15, Dec. 2021.

[b] A. Naikoti and A. Chockalingam, "Signal detection and channel estimation in OTFS," ZTE Communications, vol. 19, no. 4, pp. 16–33, Dec. 2021.

[c] T. Thaj and E. Viterbo, "Low complexity Iterative Rake Decision Feedback Equalizer for Zero-Padded OTFS systems,"in *IEEE Trans. Veh. Tech.*, vol. 69, no. 12, pp. 15606-15622, Dec. 2020, doi: 10.1109/TVT.2020.3044276.

Weakness of the MP detection

- The number of delay-Doppler domain paths P is very high in practical cases.
- Complexity of message passing detection scales linearly with P.
- Complexity of message passing detection also scales linearly with modulation size Q, implying it incurs high complexity for high order modulation.

Maximal Ratio Combining Detection

- Detection complexity comparable to single tap equalizer
- Performance similar to MP detector
- Ease of implementation
- We discuss MRC for zero padded (ZP) OTFS since ZP can be used as guard symbols for pilot.
- Can be easily extended to other OTFS variants
- Detailed introduction is available in:

the IEEE ComSoc Training Course, 16 - 17 November 2022, 2:00 pm to 6:00 pm EST, Viterbo (Instructor), Hong and Thaj (Developers)

https://www.comsoc.org/education-training/training-courses/online-courses/2022-11-otfs-and-delay-doppler-communications

OTFS Parameters

Parameter	Value
Carrier frequency	4 GHz
No. of subcarriers (M)	512
No. of OTFS symbols (N)	128
Subcarrier spacing	15 KHz
Cyclic prefix of OFDM	2.6 μs
Modulation alphabet	4-QAM
UE speed (Kmph)	30, 120, 500
Channel estimation	Ideal

TABLE I

SIMULATION PARAMETERS

Simulation results – damping factor Δ

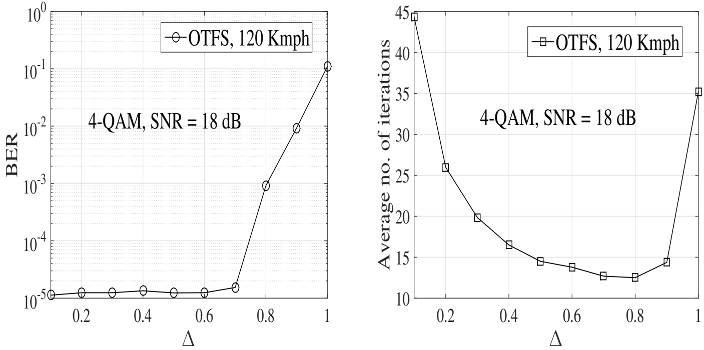

Figure: Variation of BER and average iterations no. with Δ. Optimal for $\Delta = 0.7$

Simulation results – OTFS vs OFDM with ideal pulses

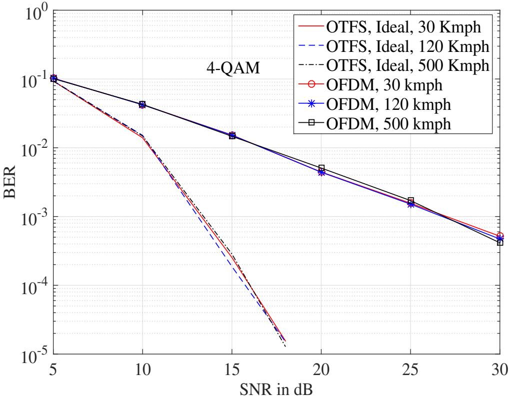

Figure: The BER performance comparison between OTFS with ideal pulses and OFDM systems at different Doppler frequencies.

Simulation results – Ideal and Rectangular pulses

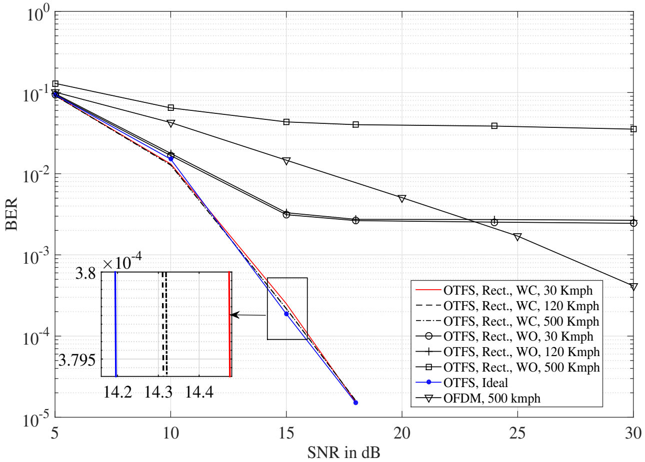

Figure: The BER performance of OTFS with rectangular and ideal pulses at different Doppler frequencies for 4-QAM.

Simulation results – Ideal and Rect. pulses - 16-QAM

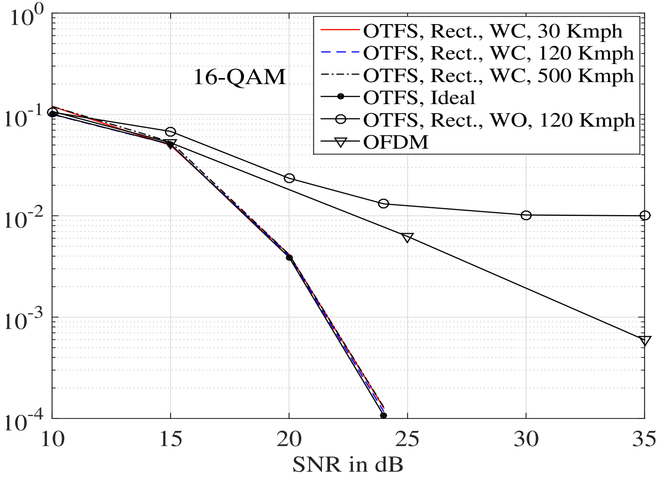

Figure: The BER performance of OTFS with rectangular and ideal pulses at different Doppler frequencies for 16-QAM.

OTFS channel estimation

Channel estimation using single pilot in the delay-Doppler domain

- Each transmit and receive antenna pair sees a different channel having a finite support in the delay-Doppler domain
- The support is determined by the delay and Doppler spread of the channel
- The OTFS input-output relation for pth transmit antenna and qth receive antenna pair can be written as

$$\mathbf{Y}^{(r)}[k,l] = \sum_{t=1}^{n_{\mathrm{T}}} \sum_{i=1}^{P^{(r,t)}} h_i^{(r,t)} \alpha(k,l,k_i^{(r,t)},l_i^{(r,t)}) \mathbf{X}^{(t)}[[[k-k_i^{(r,t)}]_N, l-l_i^{(r,t)}]_M]$$

1. P. Raviteja, K. T. Phan and Y. Hong, "Embedded Pilot-Aided Channel Estimation for OTFS in Delay–Doppler Channels" in *IEEE Transactions on Vehicular Technology*, vol. 68, no. 5, pp. 4906-4917, May 2019.
2. M. K. Ramachandran and A. Chockalingam, "MIMO-OTFS in High-Doppler Fading Channels: Signal Detection and Channel Estimation" 2018 *IEEE Global Communications Conference* (GLOBECOM), 2018, pp. 206-212.
3. R. Hadani and S. Rakib, "OTFS methods of data channel characterization and uses thereof." U.S. Patent 9 444 514 B2, Sept. 13, 2016.

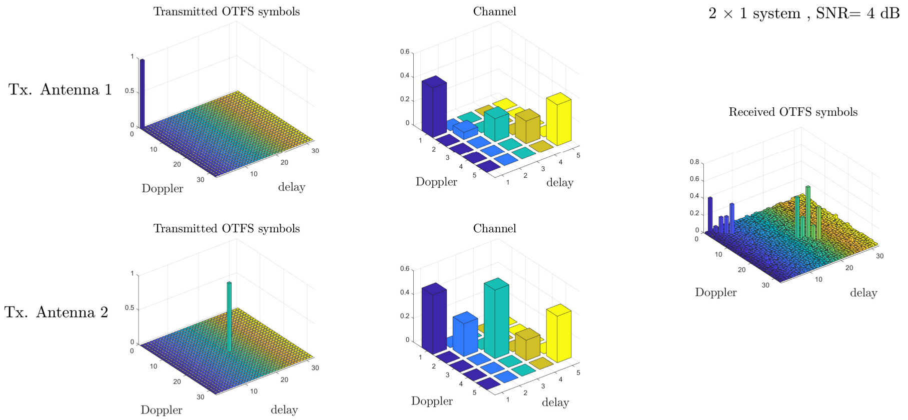

Figure: Illustration of pilots and channel response in delay-Doppler domain in a 2×1 MIMO-OTFS system

SISO OTFS system with integer Doppler

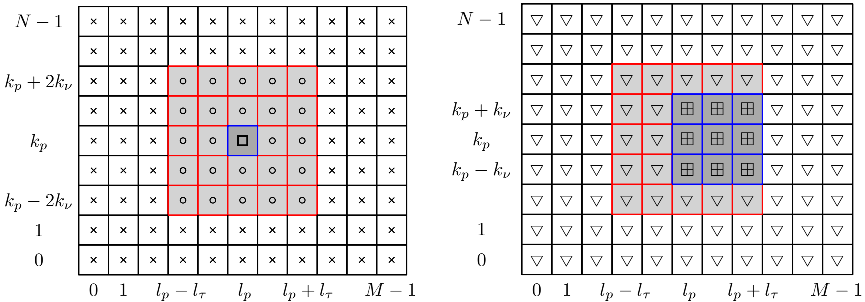

(a) Tx symbol arrangement (□: pilot; ○: guard symbols; ×: data symbols)

(b) Rx symbol pattern (▽: data detection, ⊞: channel estimation)

Figure: Tx pilot, guard, and data symbols and Rx received symbols

SISO OTFS system with fractional Doppler

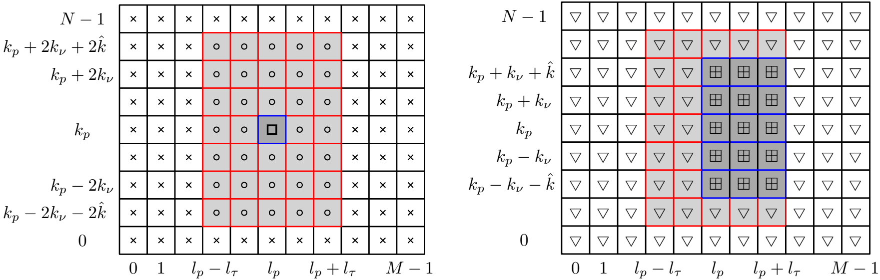

(a) Tx symbol arrangement (□: pilot; ○: guard symbols; ×: data symbols)

(b) Rx symbol pattern (▽: data detection, ⊞: channel estimation)

Figure: Tx pilot, guard, and data symbols and Rx received symbols

MIMO OTFS system

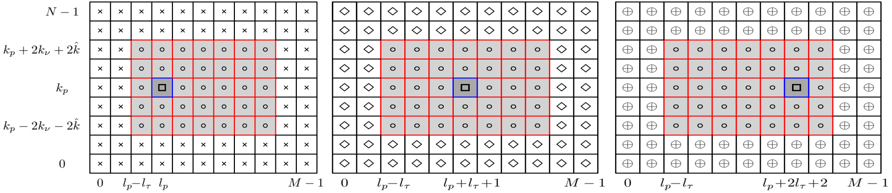

(a) Antenna 1 ($\times$: antenna 1 data symbol) (b) Antenna 2 ($\Diamond$: antenna 2 data symbol) (c) Antenna 3 ($\oplus$: antenna 3 data symbol)

Figure: Tx pilot, guard, and data symbols for MIMO OTFS system ($\square$: pilot; $\circ$: guard)

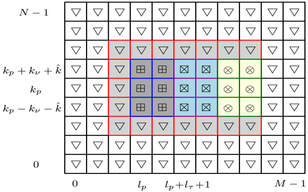

Figure: Rx symbol pattern at antenna 1 of MIMO OTFS system ($\triangledown$: data detection, $\boxplus$, $\boxtimes$, $\otimes$: channel estimation for Tx antenna 1, 2, and 3, respectively)

Multiuser OTFS system – uplink

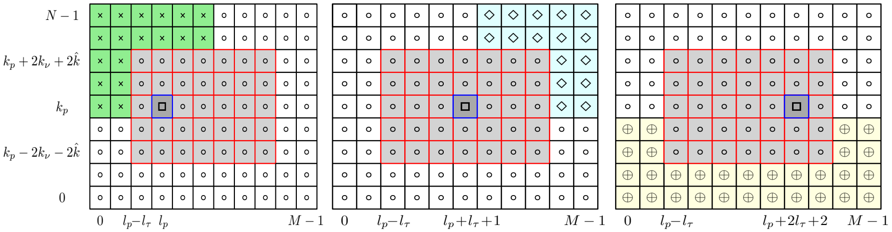

(a) User 1 (×: user 1 data symbol)

(b) User 2 (◊: user 2 data symbol)

(c) User 3 (⊕: user 3 data symbol)

Figure: Tx pilot, guard, and data symbols for multiuser uplink OTFS system (□: pilot; ○: guard symbols)

*P. Raviteja, K. T. Phan, and Y. Hong, "Embedded pilot-aided channel estimation for OTFS in delay-Doppler channels," *IEEE Trans. on Veh. Technol.*, vol. 68, no. 5, pp. 4906-4917, May 2019.

SISO-OTFS performance with the estimated channel

- Simulation parameters: Carrier frequency of 4GHz, sub-carrier spacing of 15KHz, $M = 512$, $N = 128$, 4-QAM signaling, LTE EVA channel model, and MP detection.
- Let SNR_p and SNR_d denote the average pilot and data SNRs
- Channel estimation threshold is $3\sigma_p$, where $\sigma_p^2 = 1/SNR_p$ is effective noise power of the pilot signal

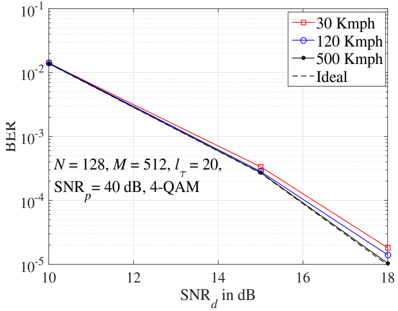

(a) BER for estimated channels of different Integer Dopplers

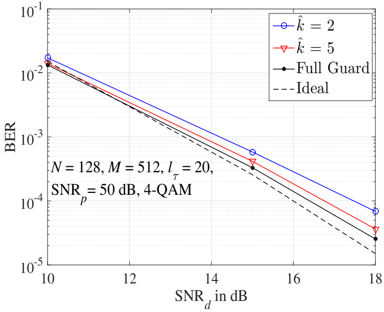

(b) BER for estimated channels of Fractional Doppler

Our recent publications

1. T. Thaj, E. Viterbo, and Y. Hong, "Orthogonal Time Sequency Multiplexing Modulation: Analysis and Low Complexity Receiver Design", *IEEE Trans. on Wireless Commun.*, vol. 20, no. 12, pp. 7842-7855, Dec. 2021.
2. T. Thaj and E. Viterbo, "Low-Complexity Linear Diversity-Combining Detector for MIMO-OTFS", *IEEE Wireless Commun. Lett.*, vol. 11, no. 2, pp. 288-292, Feb. 2022.
3. Y. Hong, T. Thaj, and E. Viterbo, *Delay-Doppler Communications: Principles and Applications.* Academic Press - Elsevier, 2/2022, ISBN:9780323850285.

OTFS in LEO Satcom

OTFS in LEO Satcom

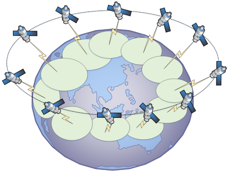

- LEO satellites circle the earth at an altitude of $500 - 2000$ km.
- LEO satellites orbit the earth at a speed of $7 - 8$ km/s
- For example, a LEO satellite's velocity at 1500km altitude is 7.1172 km/s. When $f_c = 20$GHz, the maximum Doppler shifts can be upto 400 kHz.
- Recently, OTFS-based LEO satcoms were investigated [1-4].

*A. Bora, K. Phan, Y. Hong, "Spatially Correlated MIMO-OTFS for LEO Satellite Communication Systems," *IEEE ICC Workshop on OTFS*, Seoul, 2022.
*X. Zhou, et al., "Joint Active User Detection and Channel Estimation for Grant-Free NOMA-OTFS in LEO Constellation Internet- of-Things," *2021 IEEE ICCC*, pp. 735–740, 2021.
*T. Li, et al., "OTFS modulation performance in a satellite-to-ground channel at sub-6-GHz and millimeter-wave bands with high mobility," *Frontiers of Information Technology and Electronic Engineering*, 2021.
*X. Zhou, et al., "Active Terminal Identification, Channel Estimation and Signal Detection for Grant-Free NOMA-OTFS in LEO Satellite Internet-of-Things," arXiv:2201.02084, 2022.

OTFS in LEO Satcom

- LEO satcom channel:

$$h(\tau,\nu) = \sum_{i=1}^{P} h'_i \delta(\tau - \tau_i)\delta(\nu - \nu_i)$$

- Delay taps [3GPP-TR38.901]:

$$\tau_i = \tau_{i,\mathrm{norm}} \times \mathrm{DS}_{\mathrm{desired}}$$

- $\tau_{i,\mathrm{norm}}$ is the additional delay over the first arrival delay
- $\mathrm{DS}_{\mathrm{desired}}$ is scaling parameter that makes the delay spread values span the range in channel measurements corresponding to typical 5G evaluation scenarios.

(*) "5G Study on channel model for frequencies from 0.5 to 100 GHz", (3GPP TR 38.901 version 16.1.0 Release 16), Nov. 2020.

(*) "3rd Generation Partnership Project; Technical Specification Group Radio Access Network; Study on New Radio (NR) to support non-terrestrial networks (Release 15)", 3GPP TR 38.811 V15.3.0, July 2020.

OTFS in LEO Satcom

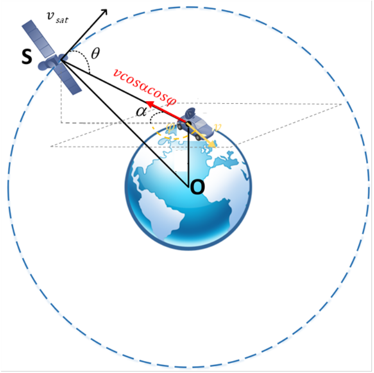

- Doppler shifts [3GPP-TR38.811]:

$$f_d = (f_c + f_{\text{sat}})\frac{v\cos\alpha\cos\varphi}{c}, \quad f_{\text{sat}} = \frac{v_{\text{sat}}}{c} f_c \cos\theta, \quad \cos\theta = \cos\alpha \frac{R}{R+h}$$

OTFS in LEO Satcom (Noiseless)

- SISO-OTFS I/O: $\mathbf{r} = \mathbf{G}\mathbf{s}$, and $\mathbf{G} = \sum_{i=1}^{P} h_i' \mathbf{\Pi}^{l_i} \mathbf{\Delta}^{(k_i)}$.
- MIMO-OTFS I/O: $\mathbf{r}_{\mathrm{MIMO}} = \mathbf{G}_{\mathrm{MIMO}} \cdot \mathbf{s}_{\mathrm{MIMO}}$

$$\mathbf{G}_{\mathrm{MIMO}} = \begin{bmatrix} \mathbf{G}^{(1,1)} & \cdots & \mathbf{G}^{(1,n_T)} \\ \vdots & \ddots & \vdots \\ \mathbf{G}^{(n_R,1)} & \cdots & \mathbf{G}^{(n_R,n_T)} \end{bmatrix} = \sum_{i=1}^{P} \underbrace{\begin{bmatrix} h_i'^{(1,1)} & \cdots & h_i'^{(1,n_T)} \\ \vdots & \ddots & \vdots \\ h_i'^{(n_R,1)} & \cdots & h_i'^{(n_R,n_T)} \end{bmatrix}}_{\mathcal{H}_i} \otimes \mathbf{\Pi}^{l_i} \mathbf{\Delta}^{(k_i)}$$

- If Rx/Tx have antenna correlations $\mathbf{R}_{\mathrm{rx}}$ and $\mathbf{R}_{\mathrm{tx}}$, whitening transformation can be applied to remove spatial correlation on channel

$$\boxed{\mathbf{r}^{c}_{\mathrm{MIMO}} = \mathbf{G}^{c}_{\mathrm{MIMO}} \cdot \mathbf{x}_{\mathrm{MIMO}}} \rightarrow \boxed{\mathbf{r}^{w}_{\mathrm{MIMO}} = \mathbf{G}_{\mathrm{MIMO}} \cdot \mathbf{x}_{\mathrm{MIMO}}}$$

(*) A. Bora, K. Phan, Y. Hong, "Spatially Correlated MIMO-OTFS for LEO Satellite Communication Systems," *IEEE ICC Workshop on OTFS*, Seoul, 2022.

Simulation Results

Parameter	Value
Earth Radius	6371Km
Sat. Height	1500Km
Elev. Angle	50°
Sat. Speed	7.11Km/h
Terminal Speed	500Km/h
Chan. Model	NTN-TDL-D

Parameter	Value
M	32
N	32
QAM	4
Sub. Spacing	240KHz
Carr. Frequency	20GHz
Detection	MP

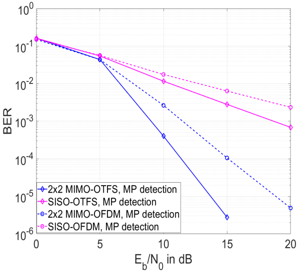

(a) OTFS vs OFDM

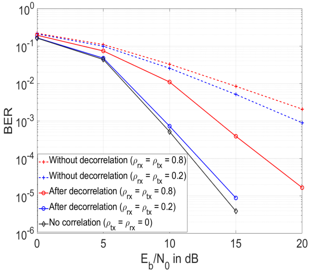

(b) MIMO-OTFS (corr. vs decorr.)

Special Thanks to

E. Viterbo, T. Thaj, A. Bora, K. Phan, and P. Raviteja

References I

1. R. Hadani, S. Rakib, M. Tsatsanis, A. Monk, A. J. Goldsmith, A. F. Molisch, and R. Calderbank, "Orthogonal time frequency space modulation," in *Proc. IEEE WCNC*, San Francisco, CA, USA, March 2017.
2. R. Hadani, S. Rakib, S. Kons, M. Tsatsanis, A. Monk, C. Ibars, J. Delfeld, Y. Hebron, A. J. Goldsmith, A.F. Molisch, and R. Calderbank, "Orthogonal time frequency space modulation," Available online: https://arxiv.org/pdf/1808.00519.pdf.
3. R. Hadani, and A. Monk, "OTFS: A new generation of modulation addressing the challenges of 5G," *OTFS Physics White Paper*, Cohere Technologies, 7 Feb. 2018. Available online: https://arxiv.org/pdf/1802.02623.pdf.
4. R. Hadani et al., "Orthogonal Time Frequency Space (OTFS) modulation for millimeter-wave communications systems," 2017 IEEE MTT-S International Microwave Symposium (IMS), Honolulu, HI, 2017, pp. 681-683.
5. A. Fish, S. Gurevich, R. Hadani, A. M. Sayeed, and O. Schwartz, "Delay-Doppler channel estimation in almost linear complexity," *IEEE Trans. Inf. Theory*, vol. 59, no. 11, pp. 7632–7644, Nov 2013.
6. A. Monk, R. Hadani, M. Tsatsanis, and S. Rakib, "OTFS - Orthogonal time frequency space: A novel modulation technique meeting 5G high mobility and massive MIMO challenges." Technical report. Available online: https://arxiv.org/ftp/arxiv/papers/1608/1608.02993.pdf.
7. R. Hadani and S. Rakib. "OTFS methods of data channel characterization and uses thereof." U.S. Patent 9 444 514 B2, Sept. 13, 2016.

References II

8. Xiang-Gen Xia, "Precoded and vector OFDM robust to channel spectral nulls and with reduced cyclic prefix length in single transmit antenna systems" in *IEEE Transactions on Communications*, vol. 49, no. 8, pp. 1363-1374, Aug. 2001, doi: 10.1109/26.939855.
9. Zak, J., "Finite Translations in Solid-State Physics", *Physical Review Letters*, vol. 19, no. 24, pp. 1385–1387, 1967. doi:10.1103/PhysRevLett.19.1385.
10. H. Bolcskei and F. Hlawatsch, "Discrete Zak transforms, polyphase transforms, and applications," in *IEEE Transactions on Signal Processing,* vol. 45, no. 4, pp. 851-866, April 1997, doi: 10.1109/78.564174.
11. Janssen, Ajem Guido. "The Zak transform : a signal transform for sampled time-continuous signals." *Philips Journal of Research*.
12. P. Raviteja, K. T. Phan, Q. Jin, Y. Hong, and E. Viterbo, "Low-complexity iterative detection for orthogonal time frequency space modulation," in *Proc. IEEE WCNC,* Barcelona, April 2018.
13. P. Raviteja, K. T. Phan, Y. Hong, and E. Viterbo, "Interference cancellation and iterative detection for orthogonal time frequency space modulation," *IEEE Trans. Wireless Commun.*, vol. 17, no. 10, pp. 6501-6515, Oct. 2018.
14. P. Raviteja, K. T. Phan, Y. Hong, and E. Viterbo, "Embedded delay-Doppler channel estimation for orthogonal time frequency space modulation," in *Proc. IEEE VTC2018-fall,* Chicago, USA, August 2018.

References III

15. P. Raviteja, K. T. Phan, and Y. Hong, “Embedded pilot-aided channel estimation for OTFS in delay-Doppler channels,” in *IEEE Transactions on Vehicular Technology*, vol. 68, no. 5, pp. 4906 - 4917, May 2019.
16. P. Raviteja, Y. Hong, E. Viterbo, and E. Biglieri, “Practical pulse-shaping waveforms for reduced-cyclic-prefix OTFS,” *IEEE Trans. Veh. Technol.*, vol. 68, no. 1, pp. 957-961, Jan. 2019.
17. P. Raviteja, Y. Hong, and E. Viterbo, “OTFS performance on static multipath channels,” *IEEE Wireless Commun. Lett.*, Jan. 2019, doi: 10.1109/LWC.2018.2890643.
18. P. Raviteja, K.T. Phan, Y. Hong, and E. Viterbo, “Orthogonal time frequency space (OTFS) modulation based radar system,” accepted in *Radar Conference*, Boston, USA, April 2019.
19. Li Li, H. Wei, Y. Huang, Y. Yao, W. Ling, G. Chen, P. Li, and Y. Cai, “A simple two-stage equalizer with simplified orthogonal time frequency space modulation over rapidly time-varying channels,” available online: https://arxiv.org/abs/1709.02505.
20. T. Zemen, M. Hofer, and D. Loeschenbrand, “Low-complexity equalization for orthogonal time and frequency signaling (OTFS),” available online: https://arxiv.org/pdf/1710.09916.pdf.
21. T. Zemen, M. Hofer, D. Löschenbrand and C. Pacher, ”Iterative Detection for Orthogonal Precoding in Doubly Selective Channels,” 2018 IEEE 29th Annual International Symposium on Personal, Indoor and Mobile Radio Communications (PIMRC), 2018, pp. 1-7, doi: 10.1109/PIMRC.2018.8580716.

References IV

22. K. R. Murali and A. Chockalingam, "On OTFS modulation for high-Doppler fading channels," in *Proc. ITA'2018,* San Diego, Feb. 2018.
23. S. Tiwari, S. Das, V. Rangamgari, "Low complexity LMMSE receiver for OTFS", IEEE communications letters, vol. 23. no. 12, pp. 2205-2209, Dec. 2019.
24. G.D. Surabhi and A. Chockalingam, "A Low-complexity linear equalization for OTFS modulation", in IEEE commun. letters, vol. 24, no. 2, pp. 330– 334, 2020.
25. M. K. Ramachandran and A. Chockalingam, "MIMO-OTFS in High-Doppler Fading Channels: Signal Detection and Channel Estimation," 2018 IEEE Global Communications Conference (GLOBECOM), 2018, pp. 206-212, doi: 10.1109/GLOCOM.2018.8647394.
26. A. Farhang, A. RezazadehReyhani, L. E. Doyle, and B. Farhang-Boroujeny, "Low complexity modem structure for OFDM-based orthogonal time frequency space modulation," in *IEEE Wireless Communications Letters,* vol. 7, no. 3, pp. 344-347, June 2018.
27. A. RezazadehReyhani, A. Farhang, M. Ji, R. R. Chen, and B. Farhang-Boroujeny, "Analysis of discrete-time MIMO OFDM-based orthogonal time frequency space modulation," in *Proc. 2018 IEEE International Conference on Communications (ICC),* Kansas City, MO, USA, pp. 1-6, 2018.
28. V. Khammammetti and S. K. Mohammed, "OTFS-Based Multiple-Access in High Doppler and Delay Spread Wireless Channels," in IEEE Wireless Communications Letters, vol. 8, no. 2, pp. 528-531, April 2019, doi: 10.1109/LWC.2018.2878740.

References V

29. B. C. Pandey, S. K. Mohammed, P. Raviteja, Y. Hong and E. Viterbo, "Low Complexity Precoding and Detection in Multi-User Massive MIMO OTFS Downlink," in IEEE Transactions on Vehicular Technology, vol. 70, no. 5, pp. 4389-4405, May 2021, doi: 10.1109/TVT.2021.3061694.
30. S. K. Mohammed, "Time-Domain to Delay-Doppler Domain Conversion of OTFS Signals in Very High Mobility Scenarios," in IEEE Transactions on Vehicular Technology, vol. 70, no. 6, pp. 6178-6183, June 2021, doi: 10.1109/TVT.2021.3071942.
31. S. K. Mohammed, "Derivation of OTFS Modulation From First Principles," in IEEE Transactions on Vehicular Technology, vol. 70, no. 8, pp. 7619-7636, Aug. 2021, doi: 10.1109/TVT.2021.3069913.
32. T. Thaj and E. Viterbo, "Low Complexity Iterative Rake Decision Feedback Equalizer for Zero-Padded OTFS Systems," in IEEE Transactions on Vehicular Technology, vol. 69, no. 12, pp. 15606-15622, Dec. 2020, doi: 10.1109/TVT.2020.3044276.
33. T. Thaj and E. Viterbo, "Low Complexity Iterative Rake Detector for Orthogonal Time Frequency Space Modulation," 2020 IEEE Wireless Communications and Networking Conference (WCNC), 2020, pp. 1-6, doi: 10.1109/WCNC45663.2020.9120526.
34. T. Thaj and E. Viterbo, "OTFS Modem SDR Implementation and Experimental Study of Receiver Impairment Effects," 2019 IEEE International Conference on Communications Workshops (ICC Workshops), 2019, pp. 1-6, doi: 10.1109/ICCW.2019.8757167.

References VI

35. T. Thaj and E. Viterbo, "Low-Complexity Linear Diversity-Combining Detector for MIMO-OTFS" in *IEEE Wireless Communications Letters*, vol. 11, no.2, pp. 288-292, Feb. 2022.
36. Y. Hong, T. Thaj and E. Viterbo, *Delay-Doppler Communications: Principles and Applications.* Academic Press, 2022, ISBN:9780323850285
37. A. Bora, K. Phan, Y. Hong, "Spatially Correlated MIMO-OTFS for LEO Satellite Communication Systems," *IEEE ICC Workshop on OTFS*, Seoul, 2022.
38. X. Zhou, et al., "Joint Active User Detection and Channel Estimation for Grant-Free NOMA-OTFS in LEO Constellation Internet- of-Things," *2021 IEEE ICCC*, pp. 735–740, 2021.
39. T. Li, et al., "OTFS modulation performance in a satellite-to-ground channel at sub-6-GHz and millimeter-wave bands with high mobility," *Frontiers of Information Technology and Electronic Engineering*, 2021.
40. X. Zhou, et al., "Active Terminal Identification, Channel Estimation and Signal Detection for Grant-Free NOMA-OTFS in LEO Satellite Internet-of-Things," arXiv:2201.02084, 2022.
41. "5G Study on channel model for frequencies from 0.5 to 100 GHz", (3GPP TR 38.901 version 16.1.0 Release 16), 2020-11.
42. "3rd Generation Partnership Project; Technical Specification Group Radio Access Network; Study on New Radio (NR) to support non-terrestrial networks", (Release 15) July 2020, 3GPP TR 38.811 V15.3.0.

References VII

43. Y. Ge, Q. Deng, P. C. Ching, and Z. Ding, "Receiver Design for OTFS With a Fractionally Spaced Sampling Approach", in IEEE Trans. on Wireless Commun., vol. 20, no. 7, pp. 4072-4086, July 2021.
44. L. Xiang, Y. Liu, L. Yang, and L. Hanzo, "Gaussian approximate message passing detection of orthogonal time frequency space modulation", in IEEE Trans. on Veh. Tech., vol. 70, no. 10, pp. 10999-11004, Oct. 2021.
45. S. Li, W.J. Yuan, Q. Wei, et al, "Hybrid MAP and PIC detection for OTFS modulation", in IEEE trans. on Veh. Tech., vol. 70, no. 7, pp. 7193–7198, July 2021.
46. H. Li, Y. Dong, C. Gong, Z. Zhang, X. Wang, and X. Dai, "Low Complexity Receiver via Expectation Propagation for OTFS Modulation", in IEEE Commun. Letters, vol. 25, no. 10, pp. 3180-3184, Oct. 2021.
47. X. Xu, M. Zhao, M. Lei, and M.J. Zhao, "A Damped GAMP Detection Algorithm for OTFS System based on Deep Learning", in Proc. of the 2020 IEEE 92nd Vehicular Technology Conference (VTC2020-Fall), Victoria, BC, Canada, pp. 1-6, Dec. 2020.
48. A. Naikoti and A. Chockalingam, "Low-complexity Delay-Doppler Symbol DNN for OTFS Signal Detection", in Proc. of the 2021 IEEE 93rd Vehicular Technology Conference (VTC2021- Spring), Helsinki, pp. 1-6, Apr. 2021. [R11]
49. Tiba. C. Zhang and S. Li, "Two-dimensional convolutional neural network based signal detection for OTFS systems", in IEEE wireless communi cations letters, vol. 10, no. 11, pp. 2514–2518.
50. Z. Zhou, L.J Liu, J.R. XU, and R. Calderbank, "Learning to equalize OTFS", available at: arxiv.org/abs/2107.08236.